Tracking heavy water (D_2O) incorporation for identifying and sorting active microbial cells

David Berry[a], Esther Mader[a], Tae Kwon Lee[a], Dagmar Woebken[a], Yun Wang[b,c], Di Zhu[c], Marton Palatinszky[a], Arno Schintlmeister[a,d], Markus C. Schmid[a], Buck T. Hanson[a], Naama Shterzer[e], Itzhak Mizrahi[e], Isabella Rauch[f], Thomas Decker[f], Thomas Bocklitz[g], Jürgen Popp[g,h], Christopher M. Gibson[i], Patrick W. Fowler[i], Wei E. Huang[c,j], and Michael Wagner[a,d,1]

[a]Division of Microbial Ecology, Department of Microbiology and Ecosystem Science and [d]Large Instrument Facility for Advanced Isotope Research, Faculty of Life Sciences, University of Vienna, A-1090 Vienna, Austria; [b]Single-Cell Center, Chinese Academy of Sciences Key Laboratory of Biofuels and Shandong Key Laboratory of Energy Genetics, Qingdao Institute of BioEnergy and Bioprocess Technology, Chinese Academy of Sciences, Qingdao, Shandong 266101, China; [c]Kroto Research Institute and [i]Department of Chemistry, University of Sheffield, Sheffield S3 7HQ, United Kingdom; [e]Department of Ruminant Sciences, Institute of Animal Science, Agricultural Research Organization, Bet-Dagan 50250, Israel; [f]Department of Microbiology, Immunobiology, and Genetics, Max F. Perutz Laboratories, University of Vienna, A-1030 Vienna, Austria; [g]Institute of Physical Chemistry and Abbe Center of Photonics, University of Jena, D-07743 Jena, Germany; [h]Institute of Photonic Technology, D-07745 Jena, Germany; and [j]Department of Engineering Science, University of Oxford, Oxford OX1 3PJ, United Kingdom

Edited by Donald E. Canfield, University of Southern Denmark, Odense M., Denmark, and approved December 3, 2014 (received for review October 27, 2014)

Microbial communities are essential to the function of virtually all ecosystems and eukaryotes, including humans. However, it is still a major challenge to identify microbial cells active under natural conditions in complex systems. In this study, we developed a new method to identify and sort active microbes on the single-cell level in complex samples using stable isotope probing with heavy water (D_2O) combined with Raman microspectroscopy. Incorporation of D_2O-derived D into the biomass of autotrophic and heterotrophic bacteria and archaea could be unambiguously detected via C-D signature peaks in single-cell Raman spectra, and the obtained labeling pattern was confirmed by nanoscale-resolution secondary ion MS. In fast-growing *Escherichia coli* cells, label detection was already possible after 20 min. For functional analyses of microbial communities, the detection of D incorporation from D_2O in individual microbial cells via Raman microspectroscopy can be directly combined with FISH for the identification of active microbes. Applying this approach to mouse cecal microbiota revealed that the host-compound foragers *Akkermansia muciniphila* and *Bacteroides acidifaciens* exhibited distinctive response patterns to amendments of mucin and sugars. By Raman-based cell sorting of active (deuterated) cells with optical tweezers and subsequent multiple displacement amplification and DNA sequencing, novel cecal microbes stimulated by mucin and/or glucosamine were identified, demonstrating the potential of the nondestructive D_2O-Raman approach for targeted sorting of microbial cells with defined functional properties for single-cell genomics.

ecophysiology | single-cell microbiology | carbohydrate utilization | nitrifier | Raman microspectroscopy

Microorganisms play a vital role in many environments. They mediate global biogeochemical cycles, catalyze biotechnological processes, and contribute to health and disease in the human body. The in situ study of microbial activity in natural and engineered ecosystems is therefore of great interest. For this purpose, several elegant methods have been established that use either transcriptional or translational activity of community members (i.e., metatranscriptomics, metaproteomics) (1–3) or the incorporation of isotopically labeled substrates into biomolecules (4–10) to infer the ecophysiology of microbes in such systems. However, these bulk techniques do not offer sufficient spatial resolution to study microbial activities at the micrometer scale. Therefore, important information can be overlooked because microbial communities are frequently spatially structured (e.g., biofilms) (11) and contain populations with life cycles (12, 13). Furthermore, even apparently identical cells in clonal populations can have strongly divergent activities (14).

Consequently, microbial ecophysiology is ideally studied also at the level of the single cell, but only a restricted number of approaches exist for determining physiological properties of individual cells in a microbial community. For example, one can observe the assimilation of radioactive or stable isotope-labeled substrates into cellular biomass using microautoradiography for the former or nanoscale resolution secondary ion mass spectrometry (NanoSIMS) or Raman microspectroscopy for the latter. These approaches can be directly combined with FISH to identify labeled organisms (15–17). However, many substrates are very expensive as isotopically labeled derivatives or are not even commercially available. Also, addition of labeled substrates easily changes the composition of the natural substrate pool, and thus potentially biases microbial community structures and functions. Furthermore, in almost all ecosystems, preferred substrates of most microbial community members are not known, highlighting the need for

Significance

Measuring activity patterns of microbes in their natural environment is essential for understanding ecosystems and the multifaceted interactions of microorganisms with eukaryotes. In this study, we developed a technique that allows fast and nondestructive activity measurements of microbial communities on a single-cell level. Microbial communities were amended with heavy water (D_2O), a treatment that does not change the available substrate pool. After incubation, physiologically active cells are rapidly identified with Raman microspectroscopy by measuring cellular D incorporation. Using this approach, we characterized the activity patterns of two dominant microbes in mouse cecum samples amended with different carbohydrates and discovered previously unidentified bacteria stimulated by mucin and/or glucosamine by combining Raman microspectroscopy and optical tweezer-based sorting.

Author contributions: D.B., D.W., and M.W. designed research; D.B., E.M., T.K.L., Y.W., D.Z., M.P., A.S., M.C.S., B.T.H., N.S., I.R., and C.M.G. performed research; I.M., T.D., T.B., J.P., C.M.G., P.W.F., and W.E.H. contributed new reagents/analytic tools; D.B., E.M., T.K.L., D.W., M.P., A.S., M.C.S., I.M., T.B., J.P., P.W.F., W.E.H., and M.W. analyzed data; and D.B., T.K.L., A.S., and M.W. wrote the paper.

The authors declare no conflict of interest.

This article is a PNAS Direct Submission.

Freely available online through the PNAS open access option.

Data deposition: The sequences reported in this paper have been deposited in the National Center for Biotechnology Information Nucleotide database (accession nos. KP055097–KP055178).

[1]To whom correspondence should be addressed. Email: wagner@microbial-ecology.net.

This article contains supporting information online at www.pnas.org/lookup/suppl/doi:10.1073/pnas.1420406112/-/DCSupplemental.

single-cell tools suitable to record the general physiological activity of microbes without prior knowledge. Microbiologists have tested fluorescent probes and stains to quantify cellular rRNA or its precursors (18, 19) and membrane potential (20) as activity measures, but cellular rRNA levels often do not correlate with activity (21) and membrane potential stains perform differently with different cell types (22). Recently, heterotrophic $^{14}CO_2$ fixation was used to infer the general activity of heterotrophic microbes semiquantitatively (23), but the extent of heterotrophic CO_2 fixation can vary widely between different species and also depends on the heterotrophic substrate used for growth (24–27). In addition, fluorescence-based methods have been developed for measuring single-cell biosynthesis of macromolecules (28–30), but the generalizability and usability of these new methods, which rely on the addition of substrates with modified functional groups, are still either largely untested in complex ecosystems or have known biases across different species.

In this study, we aimed at developing a universally applicable technique that (*i*) allows one to measure the activity of individual microbes within complex samples without prior knowledge of their physiology and without altering the natural substrate pool, (*ii*) can be combined with FISH to identify cells in situ, but (*iii*) can also be performed on living cells to facilitate postmeasurement analyses like single-cell genomics or cultivation. For this purpose, we explored the suitability of heavy water [deuterium oxide (D_2O)] as an additive to microbial communities. In all known lipid biosynthesis pathways, hydrogen from water is incorporated during the reductive steps of fatty acids synthesis (31–33). Interestingly, deuterium (D) can be used in lieu of hydrogen (H) during lipid biosynthesis, leading to deuterated lipids of active microbial community members after incubation with heavy water [in natural waters, the concentration of deuterium relative to hydrogen is at very low levels of ∼0.0156% (34)]. This effect has been exploited on the bulk level to monitor lipid biosynthesis of microbes in the environment (35, 36). In addition to lipid labeling, proteins of active community members will become deuterated, as demonstrated by metaproteomics (37). Here, we show that deuterium incorporation into individual active microbial cells can easily be detected within seconds by nondestructive Raman microspectroscopy and that the amount of deuterium labeling can reliably be quantified. In proof-of-principle experiments using mouse cecal microbial communities, we combined this simple and fast technique with FISH to demonstrate the activity of *Bacteroides acidifaciens* and *Akkermansia muciniphila* to addition of four different substrates. Furthermore, we identified novel microbes stimulated by glucosamine and mucin by combining Raman microspectroscopy with optical tweezer-based sorting, multiple displacement amplification (MDA), and 16S rRNA gene sequencing.

Results and Discussion

Raman Microspectroscopy Reveals Incorporation of Deuterium from D_2O in Active Microbial Cells. Raman microspectroscopy produces a chemical "fingerprint" of the abundant molecular bonds in individual microbial cells. Because bulk analyses have demonstrated significant incorporation of D into the biomass of cells growing in the presence of heavy water (35, 37), we hypothesized that this incorporation might be detectable as a general metabolic activity marker in Raman spectra of single microbial cells. Indeed, Raman spectra of *Escherichia coli* cultivated in growth water with no, partial, or complete substitution with heavy water exhibited several distinctive shifts (Fig. 1 *A* and *B*; an overview of all experiments in this study is provided in *SI Appendix*, Table S1). Most dramatically, a broad peak appeared in a region between 2,040 and 2,300 cm^{-1} that typically has no detectable peaks in Raman spectra of non–deuterium-labeled *E. coli* cells or cells from other microbes. Furthermore, the intensity of the prominent C-H peak (between 2,800 and 3,100 cm^{-1}) was reduced with increasing D incorporation (Fig. 1 *A* and *B*). C-D_X bonds of various types, including C-D_2 and symmetrical and asymmetrical C-D_3 bonds originating from various biomolecules, reportedly produce Raman bands between 2,013 and 2,300 cm^{-1} (38–44). Furthermore, modeling of the Raman peaks induced by the C-D_X bond using deuterated palmitic acid as the model compound also predicted peaks in this region (*SI Appendix*, Fig. S1). This spectral pattern reflects a substitution of C-H_X by C-D_X in newly synthesized macromolecules in the presence of heavy water, and it is safe to assume that an important fraction of the D incorporation is found in lipids, which contribute roughly 25–30% to total cellular C-H (45, 46). Lipids from autotrophic and heterotrophic organisms show a predominance of water-derived protons (or D^+ in the presence of heavy water) (33, 35, 47) as protons from water are transferred to NAD(P) during its reduction, and these protons are then incorporated into lipids via the known fatty acid biosynthesis pathways (31–33). D will, of course, also be incorporated to some extent via other processes, such as amino acid and carbohydrate biosynthesis (37, 48). Importantly, however, control experiments with paraformaldehyde-fixed cells demonstrated that abiotic H-D exchange reactions, such as occur in amide bonds of proteins (49) or other O- and N-bound H (32), do not contribute measurably to the C-D peak region (*SI Appendix*, Fig. S2), and therefore that C-D peaks in the Raman spectrum after growth of microbes in deuterated water are exclusively caused by biological processes.

Using a supervised statistical method (principal components analysis in combination with linear discriminant analysis), a classification model was built for the presence or absence of D_2O in the growth water of *E. coli*. Using a 10-fold cross-validation scheme, the accuracy of the model was estimated to be 98%. This result indicates that Raman spectra are characteristic of growth in D_2O and an automatic discrimination based on a classification model is possible at all tested concentrations of D_2O in the growth medium (Fig. 1 and *SI Appendix*, Table S2). To quantify the deuterium content of the *E. coli* cells from growth experiments with different amounts of heavy water, the cells were subjected to NanoSIMS (Fig. 1*C*). As expected, the cellular D content was consistently lower than the D_2O concentration of the growth water (Fig. 1*D*), which is because H from organic substrates in the medium is also incorporated into the biomass during heterotrophic growth of *E. coli*. Although there was a clearly linear correlation ($R^2 = 0.84$) between the concentration of deuterated water in the growth medium and the deuterium content of the biomass, there was also some heterogeneity in the amount of incorporated deuterium between individual cells, especially at higher concentrations of deuterated water (Fig. 1*D*). This latter finding reflects physiological heterogeneity, which might be particularly pronounced at higher D_2O concentrations due to their potential inhibiting effect (below).

In the next step, several bacterial and archaeal reference strains with differing physiologies were grown as pure cultures in the presence of different amounts of D_2O. The strains included heterotrophic bacilli (*Bacillus thuringiensis* and *Bacillus subtilis*), an autotrophic nitrite-oxidizing bacterium (*Nitrospira moscoviensis*), an autotrophic ammonia-oxidizing archaeon (*Nitrosophaera gargensis*), and autotrophic methanogenic archaea (*Methanobrevibacter smithii* and *Methanocorpusculum labreanum*). These species were selected to represent a wide range of phylogenetic and physiological diversity. Again, single-cell Raman spectra of all tested strains were marked by a peak appearing in the C-D region and a reduction in the C-H peak (Fig. 2*A*), indicating that this labeling strategy can be applied across diverse organisms. As expected heterotrophic organisms showed a weaker D incorporation than autotrophically growing microorganisms, which must reduce CO_2 to produce biomass, and therefore incorporate more hydrogen atoms from water (ANOVA, $P < 0.0.001$; Fig. 2*B* and *SI Appendix*, Fig. S6). The reduced D/(D + H) of measured autotrophs compared with growth water is at least partly caused by the large D/H fractionation by autotrophs, as has been observed, for example, in methanogenic sediments (50). Furthermore, for the slow-growing reference

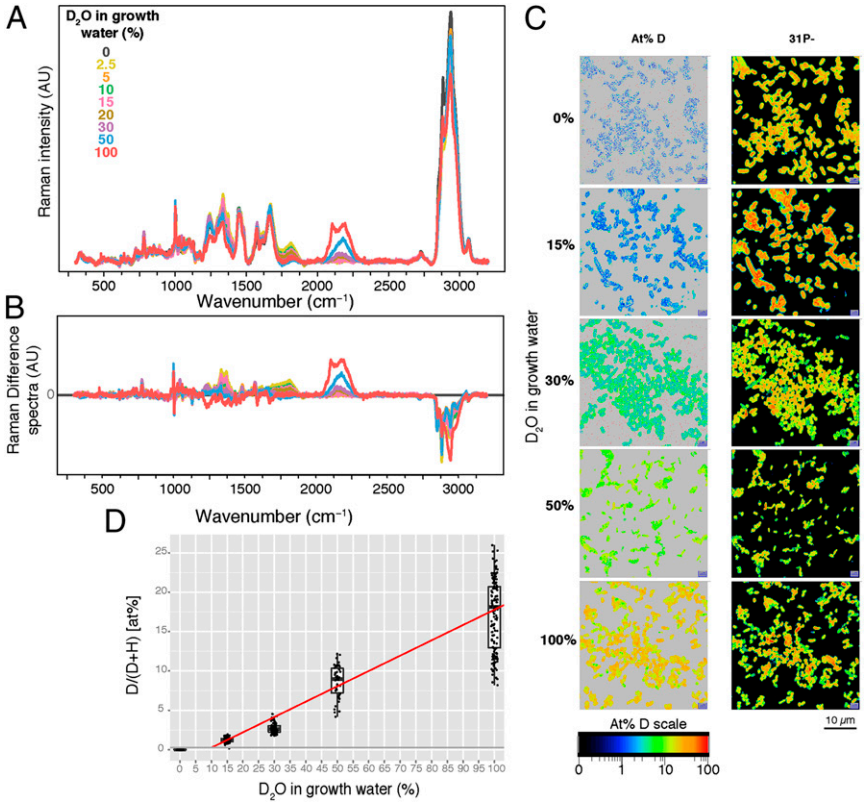

Fig. 1. *E. coli* incorporation of D from heavy water during growth as detected by Raman microspectroscopy and NanoSIMS. (*A*) Raman spectra of single *E. coli* cells grown to stationary phase in media with heavy water (0%, 2.5%, 5%, 10%, 15%, 20%, 30%, 50%, and 100% D_2O of growth water). Ten to 21 single-cell spectra were used to produce mean spectra. It should be noted that identical peak shifts were observed in *E. coli* cells that were grown in the presence of deuterated glucose instead of heavy water (*SI Appendix*, Fig. S11). AU, arbitrary unit. (*B*) Difference between mean spectra of *E. coli* cells from D_2O-containing media and cells grown without D_2O. Colors are the same as in *A*. (*C*) Quantification of D incorporation in individual *E. coli* cells from the same experiment as detected by NanoSIMS and shown as the isotope fraction D/(H + D) given as at%. All isotope fraction images are on the same scale (0–100 at%). $^{31}P^-$ signal intensity distribution is displayed to indicate the location of cellular biomass. (*D*) Comparison of D content in single cells measured by NanoSIMS with respect to the D_2O percentage of growth water. Box plots show the quartiles for each population of cells. The detection limit, defined as the mean + 3 SD of unlabeled cells, is shown in gray (0.17 at%). A linear regression between D_2O concentration and cellular D is shown in red ($R^2 = 0.84$).

organisms used in our experiments, the applied incubation time might have been insufficient to achieve complete labeling.

Although it is widely used in low doses for physiological studies (51), heavy water is known to inhibit cellular processes in mammals at higher concentrations (52). For bacteria, different responses of deuterated water on growth ranging from no effect to inhibition and even stimulation have been reported (53, 54). In our experiments, heavy water up to a concentration of 50% D_2O did not inhibit the growth of our test strains. However, the presence of 100% D_2O in the growth medium significantly reduced the specific growth rate of exponentially growing *E. coli* and *B. thuringiensis* ($P = 0.002$ and $P = 0.02$, respectively) but did not significantly affect the growth of *B. subtilis* (*SI Appendix*, Fig. S3 *A–C*). Additionally, the ammonia oxidation activity of *N. gargensis* was only slightly affected in the initial phase of incubation by up to 50% D_2O (*SI Appendix*, Fig. S3*D*), but 100% D_2O fully inhibited its growth. Taken together, these data suggest that heavy water up to 50% of total growth water can be applied in labeling studies of natural microbial communities without causing major changes in the activity of individual community members.

Raman spectra of microbial cells vary between different taxa (55, 56), and even between individual cells of the same microbial strain that have experienced different growth conditions (57), because they reflect the cellular chemical composition. Consequently, using information from the entire Raman spectrum to quantify cellular C-D abundance of a microbial cell in a complex sample will not be trivial if the study is not focused on a specific strain and sufficiently defined growth conditions. Thus, we were interested in determining if the C-D and C-H signature regions alone could be used to quantify the amount of cellular deuterium incorporation. The metric "%CD" was defined as the integrated spectral intensity of the C-D signature region as a percentage of the integrated spectral intensity of both the C-D and C-H signature regions defined above. Repeated measurement of single cells revealed that the %CD quantification was reproducible and varied much less than the variation observed within a clonal population of cells (relative SD = 0.09; *SI Appendix*, Fig. S4). Remarkably, in fast-growing *E. coli* cells in the presence of 40% D_2O, some labeled cells could already be detected by Raman spectroscopy after 20 min of incubation, demonstrating that this approach is very sensitive and does not necessarily require cell division (cell doubling time was 47 min), because synthesis of macromolecules already leads to deuterium incorporation (*SI Appendix*, Fig. S5). The %CD was linearly associated with the percentage of D_2O in the growth water for each given strain, and for all strains, the inferred detection limit (mean + 3 SD of unlabeled cells) was less than 8%CD. (*SI Appendix*, Fig. S6).

Measurement of deuterium incorporation on a single-cell level by Raman microspectroscopy can also be directly combined with FISH. Probed cells were identified using the fluorescence microscope attached to the Raman microspectrometer, and high signal-to-noise Raman spectra of such cells could be consistently recorded (*SI Appendix*, Fig. S7). The standard storage conditions used for FISH did not significantly affect %CD (*SI Appendix*, Fig. S8),

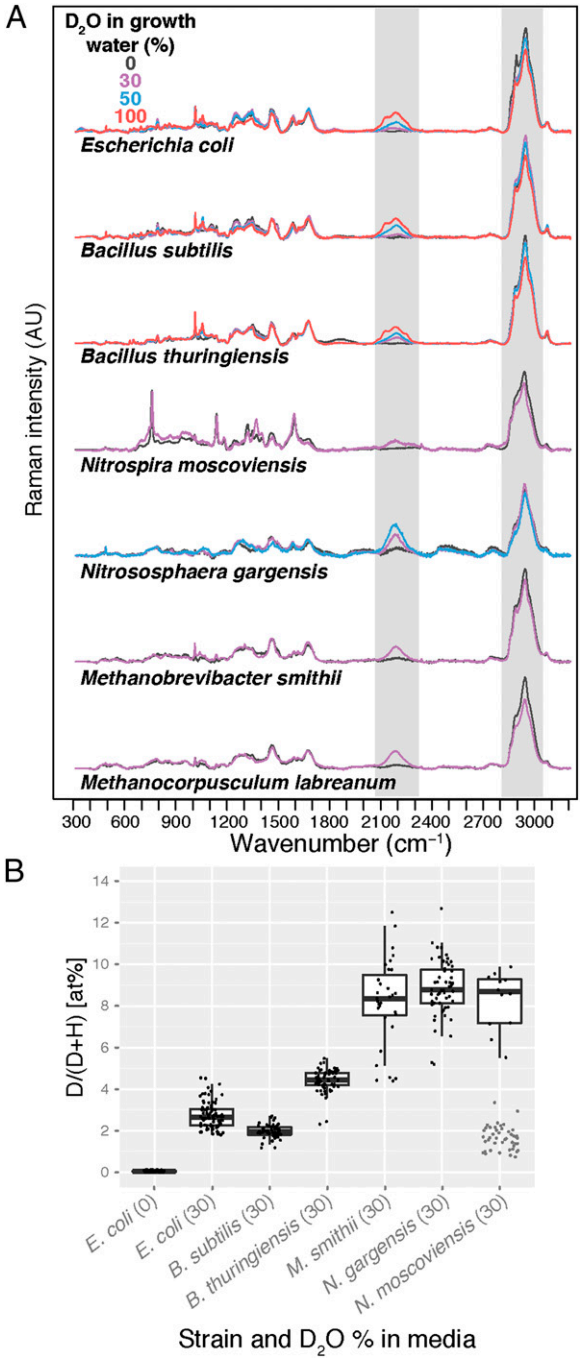

Fig. 2. C-D signature region of Raman spectra is conserved in diverse microorganisms. (*A*) Representative Raman spectra of microorganisms cultivated in media amended with various percentages of heavy water. Characteristic C-D and C-H regions are shaded in gray. *N. moscoviensis* and *N. gargensis* did not grow with 100% D_2O. Both methanogens were only grown at 30% D_2O and not tested at other levels. (*B*) NanoSIMS quantification of cellular D incorporation (at%) of different strains when grown in 30% D_2O (and *E. coli* with 0% D_2O). Each point is a measurement of a single cell, and box plots indicate quartiles. Note that only a few cells of *N. moscoviensis* became active after incubation (low-active/nonactive cells are shown in gray), a feature we have also observed by other techniques in medium without heavy water. *M. smithii* cultures produced extracellular substances enriched in D that were excluded from the analysis. Autotrophic organisms (*M. smithii*, *N. gargensis*, and *N. moscoviensis*) were significantly more enriched in D than heterotrophic organisms (*E. coli, B. subtilis*, and *B. thuringiensis*) when cultivated in the presence of the same D_2O concentration (30% D_2O; ANOVA, $P < 0.001$).

but hybridization conditions used for FISH did have an effect, leading to an average reduction in %CD by 42% (*SI Appendix*, Fig. S9). Loss of cellular D will increase the deuterium detection limit of the Raman method, which is most relevant for experiments using very low-percentage additions of heavy water or for targeting microbes with a low activity. It should be noted that some loss of labeled compounds is also expected or has already been reported in all other single-cell isotope labeling methods, for example, microautoradiography or NanoSIMS for isotope detection if either is combined with FISH or catalyzed reporter deposition (CARD)-FISH (58, 59).

Determining Compound Utilization Patterns of Members of the Gut Microbiota. The gut microbiota is important to human and animal health and nutrition (60, 61). Competition for nutrients is thought to shape the overall composition of the gut microbiota as well as the colonization success of enteropathogens (62, 63). For example, the availability of mucosally derived sugars has been shown to be a key factor in the colonization of *E. coli*, *Salmonella typhimurium*, and *Clostridium difficile* (64, 65). Although important, the compound utilization activities of individual microbes in the complex gut community are not well understood (66). In a proof-of-principle experiment, we applied the heavy water labeling approach to study how microbes in a complex microbial community respond to the addition of different nutrients with single-cell resolution. Mouse cecum contents were incubated anaerobically in the presence of 50% D_2O and were amended with sugars that are components of dietary- and/or host-derived polysaccharides (glucose, glucosamine, and mannose) or a secreted mucosal glycoprotein with mixed glycans (porcine gastric mucin) as a model complex substrate. Subsequently, single microbial cells were probed by Raman microspectroscopy for deuterium incorporation. This probe was done either by a nontargeted approach of random selection of cells or by targeted FISH-based profiling of two important degraders of host-derived compounds, *A. muciniphila* and *B. acidifaciens* (67–69) (Fig. 3*A*).

Overall, a large percentage of the cecal microbial community was stimulated by addition of glucose (81%), mannose (75%), and mucin (71%), whereas the response to glucosamine was lower (41%) (Fig. 3*B*). Additionally, a fraction of the community (~9%) was active in the incubation without substrate addition, and thus thrived due to endogenous metabolism or on decay products of other microbes. The *B. acidifaciens* population was stimulated to the greatest extent by mannose, followed by mucin, glucose, glucosamine, and, lastly, no amendment ($P < 0.05$; Fig. 3*B*). In contrast, the *A. muniphila* population was stimulated primarily by mucin, with much lower activity in mannose and glucose amendments and no increase in activity due to glucosamine compared with no amendment controls ($P < 0.05$). *B. acidifaciens* and other *Bacteroides* spp. are capable of fermenting a wide range of simple and complex carbohydrates and using mixed substrates (70–74). Previous studies have shown that in pure culture, members of the *Bacteroides* prioritize mannose utilization over other sugars (74, 75), and our results suggest that mannose may be a preferred substrate in vivo as well. Both *B. acidifaciens* and *A. muciniphila* were stimulated by mucin. These two species are known to degrade mucin in pure cultures (76, 77) and are important host-compound degraders in vivo (68). *A. muciniphila* has a phosphotransferase transporter system that is likely capable of taking up a range of simple sugars, including glucose, glucosamine, and mannose (78). Interestingly, however, this organism was stimulated in situ almost exclusively by mucin (Fig. 3 *C* and *D*). This result reinforces the concept that in vivo, *A. muciniphila* is primarily active as a mucin degrader (67) in contrast to *B. acidifaciens*, which is more versatile in its nutrient utilization strategy. The flexible foraging activity of *B. acidifaciens* raises the possibility that the presence of alternative nutrients could modify its activity in degrading host-derived compounds in

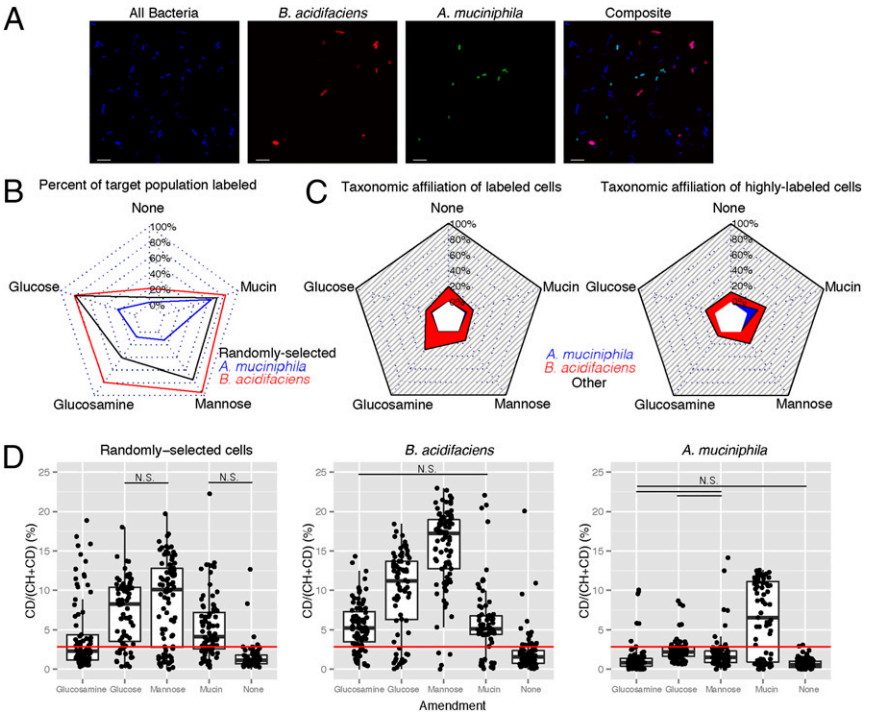

Fig. 3. Application of D_2O to monitor the activity of mouse cecum microbiota on a single-cell level after in vitro incubation with various unlabeled substrates. Experiments were performed on cecal biomass amended with glucose, glucosamine, mannose, mucin, or nothing and were incubated overnight. (*A*) Representative FISH images of all *Bacteria* (blue), *B. acidifaciens* (red), *A. muciniphila* (green), and composite. (Scale bar: 5 μm.) (*B*) Percentage of cells from the respective target population for which a C-D peak could be detected by Raman microspectroscopy under each incubation condition. For each target and incubation condition, 68–92 cells were measured. (*C*) Contributions of *B. acidifaciens* and *A. muciniphila* to all labeled (*Left*) and highly labeled (*Right*, >10% CD) cells in the gut community in the different experiments are displayed. These contributions were calculated as follows: [Relative abundance of target population as measured by quantitative FISH using a specific probe] * [Proportion of target population labeled]/[Relative abundance of all labeled cells]. (*D*) Intensity of deuterium incorporation in single cells of randomly selected (DAPI-positive) and specific FISH probe-defined populations, measured by %CD. Single-cell spectra are denoted by black points, and population quartiles are shown as box plots. The red horizontal line at 2.78%CD indicates the threshold for considering a cell labeled. It was determined by calculating the mean + 3 SD of %CD in randomly selected cells from the cecum sample that were incubated without addition of heavy water. All comparisons are statistically significantly ($P < 0.05$), except for those comparisons denoted by a black bar connecting them and labeled by N.S. (not significant).

the gut. Future research is needed to determine how this versatile foraging behavior might affect the mucus layer and if altered mucus degradation due to changed foraging patterns has an impact on immunological tolerance to the gut microbiota. By combining quantitative FISH with quantification of active cells using the Raman-based detection of deuterated cellular compounds, it could be demonstrated that *B. acidifaciens* represented an important but not dominant fraction of all highly labeled cells for all amendments (7–19% of all cells that had >10%CD), whereas *A. muciniphila* accounted for less than 1% of highly labeled cells under all conditions except for the mucin amendment, in which it represented 15% of highly labeled cells (Fig. 3*C*). These quantitative inferences demonstrated that although *B. acidifaciens* and *A. muciniphila* contributed to community activity, other unidentified microbes dominated the active microbial community after amendment of the various substrates.

Identifying Active Cells Using Raman-Based Sorting and DNA Sequencing. To demonstrate the power of heavy water labeling with Raman as a discovery tool, we further investigated cells that were highly labeled by deuterium after glucosamine (16% of all cells in the community) and mucin (9% of all cells in the community) amendments. Nonfixed samples from the incubations were directly added to a microcapillary and single cells were trapped with an optical tweezer (79) for determining their deuterium content via Raman microspectroscopy. Because neither H_2O nor D_2O has Raman peaks in the C-D region, background from water did not interfere in this approach (80). From each incubation, 40 cells with a high C-D peak (corresponding to the top decile of labeled cells) were identified and sorted by moving them individually to the sterile end of the capillary (representative spectra are shown in Fig. 4*A*). After MDA, the sorted cells were identified by 16S rRNA gene amplification, cloning, and sequencing (Fig. 4 and *SI Appendix*, Fig. S10). The obtained 16S rRNA gene sequences reflect the diversity of the substrate-stimulated cells, but it should be kept in in mind that due to well-described biases of the analysis pipeline (cell lysis, MDA, PCR, and cloning) (81), the number of clones recovered may not reflect the relative abundance of active cells in the sample. Several taxa (*Akkermansia*, *Allobaculum*, *Bacteroides*, *Barnesiella*, *Clostridiales*, *Desulfovibrioaceae*, and *Parabacteroides*) were found among the sorted cells from both incubations, demonstrating that these microbes responded to both added substrates. Many of these taxa are saccharolytic, although glucosamine and mucin utilization has not been demonstrated before for most of them (82–85). Consistent with the experiments depicted in Fig. 3, active *A. muciniphila* cells also belonged to this group. Although quantitative inferences from obtained clone numbers have to be interpreted with great caution, it is interesting to note that 15 of 39 clones were affiliated with *A. muciniphila* in the mucin incubation experiment, whereas only two of 43 clones belonged to this important mucin degrader after glucosamine incubation (Fig. 4*B*). The detection of multiple *Bacteroides* populations stimulated by mucin suggests that multiple *Bacteroides* species in the same community respond to the same compound, which

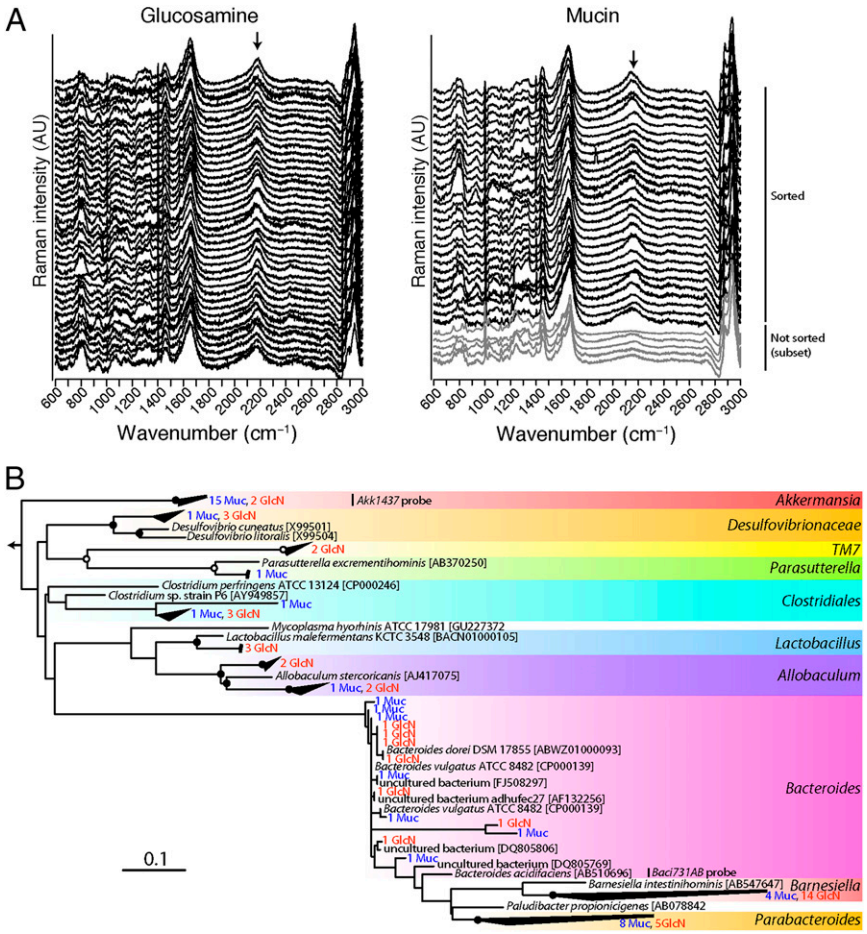

Fig. 4. Targeted sorting and phylogenetic analysis of deuterium-labeled cells from two gut microbiota incubations. (*A*) Raman spectra of 40 highly labeled cells from the glucosamine and mucin incubations, respectively, that were sorted using optical tweezers. Arrows indicate the strong C-D peaks in the spectra of the sorted cells. A few representative spectra from cells that were not sorted from the mucin incubation are also shown in gray to allow for comparison. (*B*) Phylogenetic analysis of partial 16S rRNA gene sequences recovered from sorted cells [the number of sequences is indicated and colored blue for mucin (Muc) incubation and red for glucosamine (GlcN) incubation]. The tree was produced using near-full-length sequences from organisms closely related to clone sequences (indicated in black) using RAxML with 500 bootstrap resamplings (black circles indicate >90% support, white circles indicate >75% support). Clone sequences were then added to the tree using the quick-add parsimony method in ARB. The taxonomic classification of sequences is indicated. Coverage of *A. muciniphila* and *B. acidifaciens* FISH probes (estimated from full-length sequences) is indicated. The scale bar indicates the number of substitutions per site. A fully expanded tree is presented in *SI Appendix*, Fig. S10.

could indicate either cooperative degradation of or competition for host-derived substrates among members of this genus. Future work is needed to unravel the nature of possible interactions among different *Bacteroides* species in the gut microbiota. The detection of active *Lactobacillus* cells after glucosamine detection confirms the notion that the use of this substrate is an important strategy of these microbes for survival in the gut (86). Interestingly, members of the less well-characterized TM7 candidate phylum, which were recently postulated to be saccharolytic (87), were also active after glucosamine addition. Putatively sulfate- or sulfite-reducing Desulfovibrionaceae responded to glucosamine and mucin amendments. This response likely reflects indirect stimulation of this group due to cooperative interactions with saccharolytic bacteria that produce metabolic substrates for these sulfur-compound reducers (88).

Conclusions and Outlook

This study shows that incubation of samples containing complex microbial communities with heavy water subsequently allows microbiologists to identify individual metabolically active bacterial and archaeal cells by Raman microspectroscopy without any further sample pretreatment. The C-D signature peak for deuterium incorporation into single microbial cells is easily detectable and is already visible in rapidly growing cells after 20 min of incubation. Compared with many other isotope-labeled substrates, heavy water is inexpensive and its addition to samples enables functional studies of microbial communities with minimal perturbation of the natural environmental conditions. Interestingly, the tested microbial strains showed no significant change in growth rate in the presence of up to 50% D_2O, and because much lower D_2O concentrations were sufficient for Raman-based activity measurements, toxicity of heavy water is not a limiting factor for the application of this technique. As demonstrated with incubation experiments using mouse cecum microbial communities (Fig. 3), heavy water labeling can be combined with the addition of unlabeled substrates to investigate which members of a microbial community are stimulated by which compound. This approach is particularly important for those researchers interested in the metabolic conversion of substrates that are not commercially available as isotope-labeled derivatives or for which isotope labeling is extremely expensive.

Heavy water could also be used to label microbial cells living within or attached to plants, animals, and possibly even humans. Although consumption of high amounts of heavy water is toxic or

even lethal to plants, animals, and humans (89), the D_2O concentrations required for activity labeling of microbial communities inferred in this study are below the toxicity threshold for body water deuteration of several important model animals. For example, mice and rats have been observed to be asymptomatic at D levels of 20–25% (90). Consequently, it should become possible to perform in vivo activity labeling experiments with microbial gut communities in mice by providing heavy water as drinking water for a short time period. However, the application range of the developed approach might even be much broader because it seems likely that fast-growing neoplastic cells also incorporate significantly more D from heavy water than other cells, a feature that would enable their straightforward detection via Raman microscopy or sensors (91).

Furthermore, this study demonstrated that heavy water labeling of microbial cells and Raman microspectroscopy can be combined with optical tweezing for targeted sorting of individual microbial cells with certain functional traits for subsequent characterization via MDA and DNA sequencing. Because Raman microspectroscopy and optical tweezing are nondestructive techniques that work in water, no pretreatment of the cells (other than the isotope labeling) is required; thus, this approach will not only allow single-cell genomics experiments targeted to members of defined microbial guilds but might also prove to be useful for targeted cultivation of members of microbial communities with interesting ecophysiological properties.

Materials and Methods

Microorganisms and Growth Conditions. For all strains tested, media were prepared with different percentages (vol/vol) of D_2O [99.9% atom % (at%) D; Sigma–Aldrich) to test D incorporation. Pure cultures of the Gram-negative bacterium *E. coli* DH10B and the Gram-positive strains *B. subtilis* W23 and *B. thuringiensis* American Type Culture Collection 10792 were grown aerobically in LB with shaking at 37 °C. *B. thuringiensis* was selected due to a report indicating that this species might be stimulated by D_2O (54). Fifty microliters of stationary-phase cultures was inoculated into 5 mL of LB, and growth was monitored spectrophotometrically (at 578 nm; Camspec M107 Spectrophotometer) every 30 min until stationary phase (OD at 578 nm of 0.7–0.8) to calculate the growth rate of cultures. Additionally, to determine short-term incorporation of deuterium, samples were collected at 20, 40, 60, 90, 120, 180, and 240 min. For serial growth measurements of *E. coli*, an overnight culture of cells was inoculated into fresh medium and grown overnight. For growth of *E. coli* on deuterated glucose (*SI Appendix*, Fig. S11), cells were grown in M9 medium (Sigma-Aldrich) with 10 mM of glucose as the sole carbon source. Cells were incubated with different ratios of unlabeled/deuterated glucose aerobically with shaking at 37 °C for 16 h in biological triplicate. Cells were then harvested, washed three times with deionized water, and measured with Raman microspectroscopy. *N. gargensis* was grown aerobically at 46 °C in ammonia-oxidizing archaea (AOA) medium (all chemicals from Sigma-Aldrich) (92), amended with 2 mM NH_4Cl, and regularly fed with 1 mM NH_4Cl when ammonium was depleted. Ammonium was detected by Nessler's reagent (Sigma–Aldrich), and nitrite was quantified with the sulfanilamide *N*-1-napthylethylenediamine dihydrochloride reagent spectrophotometric method (93). *N. moscoviensis* was grown in mineral medium (94) amended with 1 mM $NaNO_2$ and shaking (90 rpm, KS 4000i, IKA) at 29 °C in the dark. Nitrite was regularly checked with colorimetric test strips (Merck) and was replenished every 2 d by injection, and cultures were sampled after 6 d. The methanogen strains *Methanobrevibacter gottschalkii* (DSM 11977), *M. smithii* (DSM 861), and *M. labreanum strain Z* (DSM 4855) were grown anaerobically in Hungate tubes at 39 °C for 7 d in basal medium with vitamins according to Leahy et al. (95), including ampicillin, erythromycin, and vancomycin at 50 μg/mL. Methane production was monitored by gas chromatography (95). Cells from all bacterial and archaeal reference strains were harvested by centrifugation and fixed in 3% formaldehyde for 3 h at 4 °C and stored either in 1:1 PBS/ethanol solution or in 1:1 PBS/glycerol at −20 °C until measurement.

Mouse Cecum Incubations. All animal experiments were discussed and approved by the University of Veterinary Medicine, Vienna, Institutional Ethics Committee and conducted in accordance with protocols approved by Austrian laws (BMWF-66.006/0002-II/10b/2010). Three adult C57BL/6 mice were killed, and their ceca were harvested anaerobically in an anaerobic tent. Contents from each cecum were suspended in 7.8 mL of 50% D_2O-containing PBS and homogenized by vortexing. The homogenate was then distributed into glass vials and amended with glucose (2.5 mg/mL), glucosamine (2.5 mg/mL), mannose (2.5 mg/mL), porcine gastric mucin (1% mass/vol), or nothing (no-amendment control) (all amendment chemicals were from Sigma–Aldrich). Vials were crimp-sealed with rubber stoppers and incubated anaerobically overnight (18 h) at 37 °C without shaking. At the end of the incubation, the biomass was washed with PBS to remove D_2O and subsamples of the biomass were fixed with either 100% ethanol alone or 3% formaldehyde for 2.5 h at 4 °C and stored in 50% PBS/50% ethanol solution at −20 °C or 100% ethanol.

FISH. DNA oligonucleotide probes were used to target most bacteria (EUB338I-III mix) (96, 97), as well as the genus *Akkermansia* [Akk1437 (S-G-Akk-1437-a-A-20), 5′-CCT TGC GGT TGG CTT CAG AT-3′] (98) and *B. acidifaciens* [Baci731AB (two probes used together: S-*-Baci-0087-a-A-24, 5′-GCG CCG GTC GCC ATC AAA AGT TTG-3′ and S-*-Baci-0087-a-A-22, 5′-G CCG GTC GCC ATC GGA AGT TTG-3′), 35% formamide]. Although Akk1437 targets the entire genus *Akkermansia*, previous sequencing-based studies have shown that *A. muciniphila* is the only species of the genus in these mice (69). Probes double-labeled with either the fluorescent cyanide dye Cy3 or Cy5 (only Cy5 was used for Raman experiments) were hybridized to fixed cells of the reference strains or to fixed biomass samples at 46 °C for 2 h using a standard liquid-FISH protocol (15, 99).

Confocal Raman Microspectroscopy and Spectral Processing. Samples were spotted on aluminum-coated slides (Al136; EMF Corporation) and washed by dipping into ice-cold Milli-Q (MQ) water (Millipore) to remove traces of buffer components. Samples were stained with DAPI (1 μg/mL; Sigma–Aldrich) for 5 min and washed with MQ water. Single microbial cell spectra were acquired using either a LabRAM HR800 or an HR Evolution confocal Raman microscope (both from Horiba Jobin-Yvon) equipped with a 532-nm neodymium-yttrium aluminium garnet laser and either 300 or 600 grooves/mm diffraction grating. Spectra were acquired in the range of 400–3,200 cm^{-1}. For hybridized samples, fluorescence images of each field of view were acquired using Horiba software. Raman spectra were preprocessed as described previously (100). First, a background correction with the sensitive nonlinear iterative peak-clipping algorithm was carried out using optimized parameters (smoothing = true, iteration = 70, window = "15") (101). Thereafter, each spectrum was normalized to the sum of its absolute spectral intensity. For quantification of the degree of D substitution in C-H bonds (%CD), the bands assigned to C-D (2,040–2,300) and C-H (2,800–3,100) were calculated using integration of the specified region. Preprocessed Raman spectra were also used to construct a classification model for the presence or absence of D_2O in the growth media. Here, a principal component analysis was carried out to reduce the dimension of the data (102). Seven principal components were used to construct the classification model. As a classification model, linear discriminant analysis (103) was applied, and the predictive performance was evaluated using a 10-fold cross-validation (104). The result of this procedure can be presented in a confusion matrix, where true class labels are compared with the predicted ones. Here, these class labels are either "presence of D_2O" or "absence of D_2O."

Raman-activated cell sorting. Capillary tubes (Rectangle Glass Capillary, 0.10 × 1.00 mm; CM Scientific) were baked at 500 °C overnight before use and half-filled with sterile PBS buffer with 0.5% Tween 20. Samples from the mouse cecum incubation experiments were diluted 1:50 and introduced into capillary tubes. The end of the capillary tube at which the sample was added was sealed with petroleum jelly to prevent evaporation. The capillary tube was then placed under a 60× water immersion objective (UPlanSApo; Olympus) mounted on the Raman spectrometer. Single cells were optically trapped with a 1,064-nm laser (mpc6000; Laser Quantum), and spectra were measured over a range of 600–3,000 cm^{-1} to cover the most relevant Raman peaks in spectra of microbial cells, including the C-D peaks. When a deuterium-labeled cell was identified, it was moved to the sterile end of the capillary. After repeating this procedure for multiple labeled cells, the end of the capillary was broken off and placed in a sterile 0.2-μL tube. The lid of the tube was closed, and the sorted cells were recovered into the tube by briefly centrifuging (<10 s) with a microcentrifuge. To wash off any cells that might have stuck to the walls of the capillary, 2 μL of sterile PBS buffer was then added to the capillary piece and the tube was centrifuged again.

MDA, 16S rRNA gene clone library construction, and phylogenetic analysis. The REPLI-g Single Cell Kit (Qiagen) was used for cell lysis and MDA according to the manufacturer's instructions. MDA was performed for 8 h at 30 °C and inactivated for 3 min at 65 °C. Finally, MDA products were diluted 50-fold in sterile nuclease-free water. Bacterial 16S rRNA genes were amplified with

primers 341F (5′-CCTACGGGNGGCWGCAG-3′) and 785R (5′-GACTACHVGGGTATCTAATCC-3′) (105, 106). PCR mixtures (25 μL) contained 5 μL of diluted template, 2.5 μL of 10× Taq Buffer with KCl, 2 μL of 25 mM $MgCl_2$, 2.5 μL of 2 mM dNTP, 0.5 μL of 0.5 μM each primer, and 1 μL of Taq DNA polymerase (5 U/μL) (all reagents from Thermo Scientific). PCR analysis was performed according to the following program: 95 ° for 4 min and 35 cycles of 94 °C for 40 s, 51 °C for 30 s, and 72 ° for 1 min, with a final elongation step at 72 °C for 10 min. The PCR product was purified using the QIAQuick PCR Purification Kit (Qiagen), and a clone library was produced using the TOPO TA cloning kit (Invitrogen) according to the manufacturer's instructions. Forty-eight clones were picked from each clone library and were sent to a company (Microsynth) for Sanger sequencing. The flow grams of all 16S rRNA gene sequences were inspected manually, and only-high quality sequences were retained. Cloning vector- and primer-derived sequences were removed, and the trimmed 16S rRNA gene sequences were chimera-checked with the UCHIME program (107). All nonchimeric sequences having at least 250 nt were analyzed with ARB software and the SILVA SSU Ref NR 111 database (108). A tree was constructed from near-full-length 16S rRNA gene sequences closely related to clone sequences using the maximum likelihood method RAxML (109). Bootstrap analysis was performed (rapid bootstrap algorithm) using 500 bootstrap iterations. Clone sequences were then added to the tree using the quick-add parsimony method in ARB. Sequences have been deposited in the National Center for Biotechnology Information Nucleotide database under accession numbers KP055097–KP055178.

NanoSIMS Sample Preparation, Measurements, and Data Evaluation. Samples were deposited onto boron-doped silicon wafers (7 × 7 × 0.7 mm; Active Business Company GmbH), washed with ddH_2O, and air-dried. Measurements were carried out on a NanoSIMS NS50L (Cameca). Data were acquired by scanning a finely focused Cs^+ primary ion beam over 30 × 30–40 × 40-μm^2 areas (512 × 512 pixels and ~80-nm probe size). The primary ion beam current and the dwell time were 1.2–2.2 pA and 1.5–10 ms per (layer * pixel), respectively. The base pressure in the analysis chamber was <1.8E-10 torr, the minimized residual gas adsorption. The secondary ions $^{12}C^1H^-$, $^{12}C^2H^-$, $^{16}O^1H^-$, $^{16}O^2H^-$, $^{12}C^{14}N^-$, $^{31}P^-$, and $^{32}S^-$ were detected in parallel and with a mass resolving power of >10,000 for OH^- and CH^-. $^{16}O^1H^-$ and $^{16}O^2H^-$ or $^{12}C^1H^-$ and $^{12}C^2H^-$ were used for determination of hydrogen isotope composition. To discriminate between isobaric species, detectors were positioned to blank $^{12}CH_2^-$ and $^{16}O^1H_2^-$ selectively. The contributions of $^{13}C^1H^-$ and $^{17}O^1H^-$ were subtracted from $^{12}C^2H^-$ and $^{16}O^2H^-$ by estimating their values from $^{12}C^1H^-$ and $^{16}O^1H^-$ and multiplying by the natural abundance $^{13}C/^{12}C$ and $^{17}O/^{16}O$ values [0.0109 and 0.000380, respectively (110)]. Measurements with unlabeled *E. coli* cells were used to validate this approach, and resulted in D/(H + D) values of 0.0214 ± 0.0495 at% (1σ) and 0.0181 ± 0.0243 at% (1σ) based on CH^- and OH^- detection, respectively. These values are well within the range of natural variation and did not significantly differ from each other ($P = 0.67$) (110). Because the analytical precision of measurements was dominated by counting statistics, values obtained from the ion species with the higher intensity were used for quantification of the isotopic composition. For data intercomparison, images acquired from regions close to the center of the cells were evaluated using the WinImage software package (Cameca). Image stacks were aligned to correct for drift of the primary ion beam and/or sample stage, dead time-corrected on a per-pixel basis, and accumulated. Regions of interest (ROIs), referring to individual cells, were manually defined by $^{12}C^{14}N^-$ and $^{31}P^-$ intensity as indicators of cellular biomass and cross-checked by the topographical/morphological appearance of the sampled areas in secondary electron images. The isotope fraction D/(H + D) was calculated per pixel by

$$D/(H+D)=\frac{^{12}C^2H^-_{corr}}{\left(^{12}C^1H^-+^{12}C^2H^-_{corr}\right)} \quad \text{or} \quad D/(H+D)=\frac{^{16}O^2H^-_{corr}}{\left(^{16}O^1H^-+^{16}O^2H^-_{corr}\right)},$$

where the subscript *corr* refers to the subtraction of the intensity originating from the coeval detection of the isobaric $^{13}C^1H^-$ and $^{17}O^1H^-$ ions, respectively. Mean D/(H + D) values for each ROI were then calculated.

ACKNOWLEDGMENTS. We thank Tanja Woyke and Roman Stocker for helpful discussions and comments on the manuscript. The work was conducted under the US Department of Energy Joint Genome Institute Emerging Technologies Opportunity Program, which is supported by the Office of Science of the US Department of Energy under Contract DE-AC02-05CH11231. The work was additionally supported financially by the Austrian Science Fund (Project P26127-B20); the Vienna Science and Technology Fund (Project LS12-001); the European Research Council [Advanced Grant Nitrification Reloaded - a Single Cell Approach (NITRICARE) 294343]; the Engineering and Physical Sciences Research Council (Grant EP/H04986X/1); the Basic Science Research Program of the National Research Foundation of Korea funded by the Ministry of Education, Science, and Technology (Grant 2013R1A6A3A03065260); and the Ministry of Science and Technology of China (Grant 2011IM030100).

1. Frias-Lopez J, et al. (2008) Microbial community gene expression in ocean surface waters. *Proc Natl Acad Sci USA* 105(10):3805–3810.
2. Urich T, et al. (2008) Simultaneous assessment of soil microbial community structure and function through analysis of the meta-transcriptome. *PLoS ONE* 3(6):e2527.
3. VerBerkmoes NC, Denef VJ, Hettich RL, Banfield JF (2009) Systems biology: Functional analysis of natural microbial consortia using community proteomics. *Nat Rev Microbiol* 7(3):196–205.
4. Adamczyk J, et al. (2003) The isotope array, a new tool that employs substrate-mediated labeling of rRNA for determination of microbial community structure and function. *Appl Environ Microbiol* 69(11):6875–6887.
5. Mayali X, et al. (2012) High-throughput isotopic analysis of RNA microarrays to quantify microbial resource use. *ISME J* 6(6):1210–1221.
6. Radajewski S, Ineson P, Parekh NR, Murrell JC (2000) Stable-isotope probing as a tool in microbial ecology. *Nature* 403(6770):646–649.
7. Schwartz E (2007) Characterization of growing microorganisms in soil by stable isotope probing with $H_2{}^{18}O$. *Appl Environ Microbiol* 73(8):2541–2546.
8. Manefield M, Whiteley AS, Griffiths RI, Bailey MJ (2002) RNA stable isotope probing, a novel means of linking microbial community function to phylogeny. *Appl Environ Microbiol* 68(11):5367–5373.
9. Jehmlich N, Schmidt F, von Bergen M, Richnow HH, Vogt C (2008) Protein-based stable isotope probing (Protein-SIP) reveals active species within anoxic mixed cultures. *ISME J* 2(11):1122–1133.
10. Pan C, et al. (2011) Quantitative tracking of isotope flows in proteomes of microbial communities. *Mol Cell Proteomics* 10:M110.006049.
11. Almstrand R, Daims H, Persson F, Sörensson F, Hermansson M (2013) New methods for analysis of spatial distribution and coaggregation of microbial populations in complex biofilms. *Appl Environ Microbiol* 79(19):5978–5987.
12. Skerker JM, Laub MT (2004) Cell-cycle progression and the generation of asymmetry in *Caulobacter crescentus*. *Nat Rev Microbiol* 2(4):325–337.
13. Haider S, et al. (2010) Raman microspectroscopy reveals long-term extracellular activity of Chlamydiae. *Mol Microbiol* 77(3):687–700.
14. Ackermann M (2013) Microbial individuality in the natural environment. *ISME J* 7(3):465–467.
15. Huang WE, et al. (2007) Raman-FISH: Combining stable-isotope Raman spectroscopy and fluorescence in situ hybridization for the single cell analysis of identity and function. *Environ Microbiol* 9(8):1878–1889.
16. Wagner M (2009) Single-cell ecophysiology of microbes as revealed by Raman microspectroscopy or secondary ion mass spectrometry imaging. *Annu Rev Microbiol* 63:411–429.
17. Dekas AE, Poretsky RS, Orphan VJ (2009) Deep-sea archaea fix and share nitrogen in methane-consuming microbial consortia. *Science* 326(5951):422–426.
18. Schmid M, Schmitz-Esser S, Jetten M, Wagner M (2001) 16S-23S rDNA intergenic spacer and 23S rDNA of anaerobic ammonium-oxidizing bacteria: Implications for phylogeny and in situ detection. *Environ Microbiol* 3(7):450–459.
19. Poulsen LK, Ballard G, Stahl DA (1993) Use of rRNA fluorescence in situ hybridization for measuring the activity of single cells in young and established biofilms. *Appl Environ Microbiol* 59(5):1354–1360.
20. Maurice CF, Haiser HJ, Turnbaugh PJ (2013) Xenobiotics shape the physiology and gene expression of the active human gut microbiome. *Cell* 152(1-2):39–50.
21. Blazewicz SJ, Barnard RL, Daly RA, Firestone MK (2013) Evaluating rRNA as an indicator of microbial activity in environmental communities: Limitations and uses. *ISME J* 7(11):2061–2068.
22. Berney M, Hammes F, Bosshard F, Weilenmann H-U, Egli T (2007) Assessment and interpretation of bacterial viability by using the LIVE/DEAD BacLight Kit in combination with flow cytometry. *Appl Environ Microbiol* 73(10):3283–3290.
23. Hesselsoe M, Nielsen JL, Roslev P, Nielsen PH (2005) Isotope labeling and microautoradiography of active heterotrophic bacteria on the basis of assimilation of $^{14}CO(2)$. *Appl Environ Microbiol* 71(2):646–655.
24. Roslev P, Larsen MB, Jørgensen D, Hesselsoe M (2004) Use of heterotrophic CO_2 assimilation as a measure of metabolic activity in planktonic and sessile bacteria. *J Microbiol Methods* 59(3):381–393.
25. Feisthauer S, et al. (2008) Differences of heterotrophic $^{13}CO_2$ assimilation by *Pseudomonas knackmussii* strain B13 and *Rhodococcus opacus* 1CP and potential impact on biomarker stable isotope probing. *Environ Microbiol* 10(6):1641–1651.
26. Sorokin JI (1966) On the carbon dioxide uptake during the cell synthesis by microorganisms. *Z Allg Mikrobiol* 6(1):69–73.
27. Sorokin YI (1966) Role of carbon dioxide and acetate in biosynthesis by sulphate-reducing bacteria. *Nature* 210(5035):551–552.
28. Hatzenpichler R, et al. (2014) In situ visualization of newly synthesized proteins in environmental microbes using amino acid tagging and click chemistry. *Environ Microbiol* 16(8):2568–2590.
29. Kuru E, et al. (2012) In Situ probing of newly synthesized peptidoglycan in live bacteria with fluorescent D-amino acids. *Angew Chem Int Ed Engl* 51(50):12519–12523.

30. Dumont A, Malleron A, Awwad M, Dukan S, Vauzeilles B (2012) Click-mediated labeling of bacterial membranes through metabolic modification of the lipopolysaccharide inner core. *Angew Chem Int Ed Engl* 51(13):3143–3146.
31. Valentine DL, Sessions AL, Tyler SC, Chidthaisong A (2004) Hydrogen isotope fractionation during H_2/CO_2 acetogenesis: Hydrogen utilization efficiency and the origin of lipid-bound hydrogen. *Geobiology* 2:179–188.
32. Sessions AL, Jahnke LL, Schimmelmann A, Hayes JM (2002) Hydrogen isotope fractionation in lipids of the methane-oxidizing bacterium *Methylococcus capsulatus*. *Geochim Cosmochim Acta* 66(22):3955–3969.
33. Zhang X, Gillespie AL, Sessions AL (2009) Large D/H variations in bacterial lipids reflect central metabolic pathways. *Proc Natl Acad Sci USA* 106(31):12580–12586.
34. Friedman I (1953) Deuterium content of natural waters and other substances. *Geochim Cosmochim Acta* 4(1-2):89–103.
35. Wegener G, et al. (2012) Assessing sub-seafloor microbial activity by combined stable isotope probing with deuterated water and ^{13}C-bicarbonate. *Environ Microbiol* 14(6):1517–1527.
36. Kellermann MY, et al. (2012) Autotrophy as a predominant mode of carbon fixation in anaerobic methane-oxidizing microbial communities. *Proc Natl Acad Sci USA* 109(47):19321–19326.
37. Justice NB, et al. (2014) 15N- and 2H proteomic stable isotope probing links nitrogen flow to archaeal heterotrophic activity. *Environ Microbiol* 16(10):3224–3237.
38. Brown HC, Bowen RD, Edwards HGM, Farwell DW (2007) Raman spectroscopy of 3-(pent-1-enyl) methyl ether and selected deuterium-labelled analogues. *J Raman Spectrosc* 38:1586–1594.
39. Bryant GJ, Lavialle F, Levin IW (1982) Effects of membrane bilayer reorganizations on the 2103 cm^{-1} Raman spectral C-D stretching mode linewidths in dimyristoyl phosphatidylcholine-d_{54} (DMPC-d_{54}) liposomes. *J Raman Spectrosc* 12:118–121.
40. Bansil R, Day J, Meadows M, Rice D, Oldfield E (1980) Laser Raman spectroscopic study of specifically deuterated phospholipid bilayers. *Biochemistry* 19(9):1938–1943.
41. Hill IR, Levin IW (1979) Vibrational spectra and carbon–hydrogen stretching mode assignments for a series of n-alkyl carboxylic acids. *J Chem Phys* 70(2):842–851.
42. Percot A, Lafleur M (2001) Direct observation of domains in model stratum corneum lipid mixtures by Raman microspectroscopy. *Biophys J* 81(4):2144–2153.
43. Sagle LB, Zimmermann J, Dawson PE, Romesberg FE (2004) A high-resolution probe of protein folding. *J Am Chem Soc* 126(11):3384–3385.
44. van Manen H-J, Lenferink A, Otto C (2008) Noninvasive imaging of protein metabolic labeling in single human cells using stable isotopes and Raman microscopy. *Anal Chem* 80(24):9576–9582.
45. Bremer H, Dennis PP (1996) *Escherichia coli and Salmonella: Cellular and Molecular Biology* (American Society for Microbiology, Washington, DC), 2nd Ed, pp 1553–1569.
46. Damoglou AP, Dawes EA (1968) Studies on the lipid content and phosphate requirement of glucose-and acetate-grown *Escherichia coli*. *Biochem J* 110(4):775–781.
47. Campbell BJ, Li C, Sessions AL, Valentine DL (2009) Hydrogen isotopic fractionation in lipid biosynthesis by H_2-consuming *Desulfobacterium autotrophicum*. *Geochim Cosmochim Acta* 73:2744–2757.
48. Fischer CR, Bowen BP, Pan C, Northen TR, Banfield JF (2013) Stable-isotope probing reveals that hydrogen isotope fractionation in proteins and lipids in a microbial community are different and species-specific. *ACS Chem Biol* 8(8):1755–1763.
49. Wales TE, Engen JR (2006) Hydrogen exchange mass spectrometry for the analysis of protein dynamics. *Mass Spectrom Rev* 25(1):158–170.
50. Li C, Sessions AL, Kinnaman FS, Valentine DL (2009) Hydrogen-isotopic variability in lipids from Santa Barbara Basin sediments. *Geochim Cosmochim Acta* 73:4803–4823.
51. Gisolfi CV, Summers RW, Schedl HP, Bleiler TL, Oppliger RA (1990) Human intestinal water absorption: Direct vs. indirect measurements. *Am J Physiol* 258(2 Pt 1): G216–G222.
52. Thomson JF (1960) Physiological effects of D2O in mammals. *Ann N Y Acad Sci* 84: 736–744.
53. Lester W, Jr, Sun SH, Seber A (1960) Observations on the influence of deuterium on bacterial growth. *Ann N Y Acad Sci* 84:667–677.
54. Lu MF, Zhang YJ, Zhang HY (2013) Isotope effects on cell growth and sporulation, and spore heat resistance, survival and spontaneous mutation of *Bacillus cereus* by deuterium oxide culture. *Afr J Microbiol Res* 7:604–611.
55. Kloss S, et al. (2013) Culture independent Raman spectroscopic identification of urinary tract infection pathogens: A proof of principle study. *Anal Chem* 85(20): 9610–9616.
56. Kalasinsky KS, et al. (2007) Raman chemical imaging spectroscopy reagentless detection and identification of pathogens: Signature development and evaluation. *Anal Chem* 79(7):2658–2673.
57. Huang WE, Bailey MJ, Thompson IP, Whiteley AS, Spiers AJ (2007) Single-cell Raman spectral profiles of *Pseudomonas fluorescens* SBW25 reflects *in vitro* and *in planta* metabolic history. *Microb Ecol* 53(3):414–425.
58. Musat N, Foster R, Vagner T, Adam B, Kuypers MMM (2012) Detecting metabolic activities in single cells, with emphasis on nanoSIMS. *FEMS Microbiol Rev* 36(2): 486–511.
59. Woebken D, et al. (2014) Revisiting N2 fixation in Guerrero Negro intertidal microbial mats with a functional single-cell approach. *ISME J*, 10.1038/ismej.2014.144.
60. Tremaroli V, Bäckhed F (2012) Functional interactions between the gut microbiota and host metabolism. *Nature* 489(7415):242–249.
61. Weinstock GM (2012) Genomic approaches to studying the human microbiota. *Nature* 489(7415):250–256.
62. Freter R, Brickner H, Botney M, Cleven D, Aranki A (1983) Mechanisms that control bacterial populations in continuous-flow culture models of mouse large intestinal flora. *Infect Immun* 39(2):676–685.
63. Stecher B, Berry D, Loy A (2013) Colonization resistance and microbial ecophysiology: Using gnotobiotic mouse models and single-cell technology to explore the intestinal jungle. *FEMS Microbiol Rev* 37(5):793–829.
64. Ng KM, et al. (2013) Microbiota-liberated host sugars facilitate post-antibiotic expansion of enteric pathogens. *Nature* 502(7469):96–99.
65. Pacheco AR, et al. (2012) Fucose sensing regulates bacterial intestinal colonization. *Nature* 492(7427):113–117.
66. Koropatkin NM, Cameron EA, Martens EC (2012) How glycan metabolism shapes the human gut microbiota. *Nat Rev Microbiol* 10(5):323–335.
67. Belzer C, de Vos WM (2012) Microbes inside—From diversity to function: The case of *Akkermansia*. *ISME J* 6(8):1449–1458.
68. Berry D, et al. (2013) Host-compound foraging by intestinal microbiota revealed by single-cell stable isotope probing. *Proc Natl Acad Sci USA* 110(12):4720–4725.
69. Berry D, et al. (2012) Phylotype-level 16S rRNA analysis reveals new bacterial indicators of health state in acute murine colitis. *ISME J* 6(11):2091–2106.
70. Martens EC, et al. (2011) Recognition and degradation of plant cell wall polysaccharides by two human gut symbionts. *PLoS Biol* 9(12):e1001221.
71. Rogers TE, et al. (2013) Dynamic responses of *Bacteroides thetaiotaomicron* during growth on glycan mixtures. *Mol Microbiol* 88(5):876–890.
72. Salyers AA, O'Brien M, Kotarski SF (1982) Utilization of chondroitin sulfate by *Bacteroides thetaiotaomicron* growing in carbohydrate-limited continuous culture. *J Bacteriol* 150(3):1008–1015.
73. Tsai HH, Hart CA, Rhodes JM (1991) Production of mucin degrading sulphatase and glycosidases by *Bacteroides thetaiotaomicron*. *Lett Appl Microbiol* 13(2):97–101.
74. Degnan BA, Macfarlane GT (1995) Carbohydrate utilization patterns and substrate preferences in *Bacteroides thetaiotaomicron*. *Anaerobe* 1(1):25–33.
75. Macfarlane GT, Hay S, Macfarlane S, Gibson GR (1990) Effect of different carbohydrates on growth, polysaccharidase and glycosidase production by *Bacteroides ovatus*, in batch and continuous culture. *J Appl Bacteriol* 68(2):179–187.
76. Derrien M, Vaughan EE, Plugge CM, de Vos WM (2004) *Akkermansia muciniphila* gen. nov., sp. nov., a human intestinal mucin-degrading bacterium. *Int J Syst Evol Microbiol* 54(Pt 5):1469–1476.
77. Salyers AA, Vercellotti JR, West SE, Wilkins TD (1977) Fermentation of mucin and plant polysaccharides by strains of *Bacteroides* from the human colon. *Appl Environ Microbiol* 33(2):319–322.
78. van Passel MWJ, et al. (2011) The genome of *Akkermansia muciniphila*, a dedicated intestinal mucin degrader, and its use in exploring intestinal metagenomes. *PLoS ONE* 6(3):e16876.
79. Huang WE, Ward AD, Whiteley AS (2009) Raman tweezers sorting of single microbial cells. *Environ Microbiol Rep* 1(1):44–49.
80. Brooker MH, Hancock G, Rice BC, Shapter J (1989) Raman frequency and intensity studies of liquid H_2O, $H_2{}^{18}O$ and D_2O. *J Raman Spectrosc* 20:683–694.
81. Rinke C, et al. (2014) Obtaining genomes from uncultivated environmental microorganisms using FACS-based single-cell genomics. *Nat Protoc* 9(5):1038–1048.
82. Park S-K, Kim M-S, Roh SW, Bae J-W (2012) *Blautia stercoris* sp. nov., isolated from human faeces. *Int J Syst Evol Microbiol* 62(Pt 4):776–779.
83. Sakamoto M, Benno Y (2006) Reclassification of Bacteroides distasonis, Bacteroides goldsteinii and Bacteroides merdae as Parabacteroides distasonis gen. nov., comb. nov., Parabacteroides goldsteinii comb. nov. and Parabacteroides merdae comb. nov. *Int J Syst Evol Microbiol* 56(Pt 7):1599–1605.
84. Greetham HL, et al. (2004) *Allobaculum stercoricanis* gen. nov., sp. nov., isolated from canine feces. *Anaerobe* 10(5):301–307.
85. Sakamoto M, Lan PTN, Benno Y (2007) *Barnesiella viscericola* gen. nov., sp. nov., a novel member of the family *Porphyromonadaceae* isolated from chicken caecum. *Int J Syst Evol Microbiol* 57(Pt 2):342–346.
86. Koskenniemi K, et al. (2011) Proteomics and transcriptomics characterization of bile stress response in probiotic *Lactobacillus rhamnosus* GG. *Mol Cell Proteomics* 10(2): M110.002741.
87. Marcy Y, et al. (2007) Dissecting biological "dark matter" with single-cell genetic analysis of rare and uncultivated TM7 microbes from the human mouth. *Proc Natl Acad Sci USA* 104(29):11889–11894.
88. Newton DF, Cummings JH, Macfarlane S, Macfarlane GT (1998) Growth of a human intestinal *Desulfovibrio desulfuricans* in continuous cultures containing defined populations of saccharolytic and amino acid fermenting bacteria. *J Appl Microbiol* 85(2):372–380.
89. Katz JJ, Crespi HL (1966) Deuterated organisms: Cultivation and uses. *Science* 151(3715):1187–1194.
90. Katz JJ, Crespi HL, Hasterlik RJ, Thomson JF, Finkel AJ (1957) Some observations on biological effects of deuterium, with special reference to effects on neoplastic processes. *J Natl Cancer Inst* 18(5):641–659.
91. Matthäus C, et al. (2012) In vivo characterization of atherosclerotic plaque depositions by Raman-probe spectroscopy and in vitro coherent anti-stokes Raman scattering microscopic imaging on a rabbit model. *Anal Chem* 84(18):7845–7851.
92. Lebedeva EV, et al. (2013) Enrichment and genome sequence of the group I.1a ammonia-oxidizing Archaeon "*Ca*. Nitrosotenuis uzonensis" representing a clade globally distributed in thermal habitats. *PLoS ONE* 8(11):e80835.
93. Bassett J, Denney RC, Jeffery GH, Mendham J (1989) *Vogel's Textbook of Quantitative Chemical Analysis* (Longman, London).
94. Spieck E, et al. (2006) Selective enrichment and molecular characterization of a previously uncultured *Nitrospira*-like bacterium from activated sludge. *Environ Microbiol* 8(3):405–415.
95. Leahy SC, et al. (2010) The genome sequence of the rumen methanogen *Methanobrevibacter ruminantium* reveals new possibilities for controlling ruminant methane emissions. *PLoS ONE* 5(1):e8926.

96. Amann RI, et al. (1990) Combination of 16S rRNA-targeted oligonucleotide probes with flow cytometry for analyzing mixed microbial populations. *Appl Environ Microbiol* 56(6):1919–1925.
97. Daims H, Brühl A, Amann R, Schleifer KH, Wagner M (1999) The domain-specific probe EUB338 is insufficient for the detection of all *Bacteria*: Development and evaluation of a more comprehensive probe set. *Syst Appl Microbiol* 22(3):434–444.
98. Derrien M, Collado MC, Ben-Amor K, Salminen S, de Vos WM (2008) The Mucin degrader *Akkermansia muciniphila* is an abundant resident of the human intestinal tract. *Appl Environ Microbiol* 74(5):1646–1648.
99. Stoecker K, Dorninger C, Daims H, Wagner M (2010) Double labeling of oligonucleotide probes for fluorescence in situ hybridization (DOPE-FISH) improves signal intensity and increases rRNA accessibility. *Appl Environ Microbiol* 76(3):922–926.
100. Bocklitz T, Walter A, Hartmann K, Rösch P, Popp J (2011) How to pre-process Raman spectra for reliable and stable models? *Anal Chim Acta* 704(1-2):47–56.
101. Ryan CG, Clayton E, Griffin WL, Sie SH, Cousens DR (1988) SNIP, a statistics-sensitive background treatment for the quantitative analysis of PIXE spectra in geoscience applications. *Nucl Instrum Methods Phys Res B* 34:396–402.
102. Pearson K (1901) On lines and planes of closest fit to systems of points in space. *Philos Mag (Abingdon)* 2:559–572.
103. Fisher RA (1936) The use of multiple measurements in taxonomic problems. *Ann Eugen* 7:179–188.
104. Kohavi R (1995) A study of cross-validation and bootstrap for accuracy estimation and model selection. *IJCAI (U S)* 14:1137–1145.
105. Muyzer G, de Waal EC, Uitterlinden AG (1993) Profiling of complex microbial populations by denaturing gradient gel electrophoresis analysis of polymerase chain reaction-amplified genes coding for 16S rRNA. *Appl Environ Microbiol* 59(3): 695–700.
106. Lee SH, Malone C, Kemp PF (1993) Use of multiple 16S rRNA-targeted fluorescent probes to increase signal strength and measure cellular RNA from natural planktonic bacteria. *Mar Ecol Prog Ser* 101:193–201.
107. Edgar RC, Haas BJ, Clemente JC, Quince C, Knight R (2011) UCHIME improves sensitivity and speed of chimera detection. *Bioinformatics* 27(16):2194–2200.
108. Ludwig W, et al. (2004) ARB: A software environment for sequence data. *Nucleic Acids Res* 32(4):1363–1371.
109. Stamatakis A, Hoover P, Rougemont J (2008) A rapid bootstrap algorithm for the RAxML Web servers. *Syst Biol* 57(5):758–771.
110. de Laeter JR, et al. (2003) Atomic weights of the elements. Review 2000 (IUPAC Technical Report). *Pure Appl Chem* 75(6):683–800.